Atmos. Meas. Tech. Discuss., 7, 5491–5532, 2014
www.atmos-meas-tech-discuss.net/7/5491/2014/
doi:10.5194/amtd-7-5491-2014

Atmospheric Measurement Techniques Discussions

Assessment of the sensitivity of core/shell parameters derived using the single-particle soot photometer to density and refractive index

J. W. Taylor[1], J. D. Allan[1,2], D. Liu[1], M. Flynn[1], R. Weber[3], X. Zhang[3,*], B. L. Lefer[4], N. Grossberg[4], J. Flynn[4], and H. Coe[1]

[1]Centre for Atmospheric Science, School of Earth, Atmospheric and Environmental Sciences, University of Manchester, Manchester, UK
[2]National Centre for Atmospheric Science, University of Manchester, Manchester, UK
[3]Georgia Institute of Technology, Atlanta, GA, USA
[4]University of Houston, Houston, TX, USA
[*]now at: Department of Civil and Environmental Engineering, University of California, Davis, CA, USA

Received: 21 March 2014 – Accepted: 27 May 2014 – Published: 5 June 2014

Correspondence to: J. W. Taylor (jonathan.taylor@manchester.ac.uk)

Published by Copernicus Publications on behalf of the European Geosciences Union.

Abstract

Black carbon (BC) is the dominant absorbing aerosol in the atmosphere, and plays an important role in climate and human health. The optical properties and cloud condensation nuclei (CCN) activity of soot depend on the amounts (both relative and absolute) of BC and nonrefractory material in the particles. Mixing between these two components is often considered using a core/shell coated sphere morphology. The Single Particle Soot Photometer (SP2) is the premier instrument for reporting distributions of both core size and coating thickness. Most studies combine the SP2's incandescence and scattering data to report coating properties, but there is variation in the assumed density and refractive index of the core that are used in these calculations.

In this study we explore the sensitivity of the reported coatings to these parameters. An assessment of the coating properties of freshly-emitted, thermodenuded ambient particles demonstrated that a core density of $1.8\,g\,cm^{-3}$ and refractive index $n = (2.26 - 1.26i)$ were the most appropriate to use with ambient soot in the Los Angeles area. Using these parameters generated a distribution of shell/core ratio of 1.04 ± 0.21, corresponding to an absolute coating thickness distribution of 1.7 ± 17.5 nm. This demonstrates that using this technique the SP2 can accurately determine the mixing state (externally or internally mixed) of ambient soot, but with limited precision. Using other core parameters resulted in an offset in the coating distribution, but similar precision. For comparison, using the core parameters that resulted in the thickest coatings (on the same particles as before) generated a distribution of shell/core ratio of 1.40 ± 0.19, corresponding to an absolute coating thickness distribution of 30.3 ± 14.9 nm. Relative changes in coatings associated with secondary aerosol condensation were captured regardless of the assumed core parameters. These results must be taken into account when comparing BC coatings measured using this technique, or if using these data for optical or CCN activity calculations.

AMTD
7, 5491–5532, 2014

1 Introduction

Black carbon (BC) is a combustion-generated aerosol ubiquitous throughout the lower levels of the atmosphere. It is damaging to human health (Janssen et al., 2012) and has a warming effect on climate (Bond et al., 2013). Due to its strong absorption of visible light, BC has important effects on regional climate and meteorology near where it is emitted (Ramanathan and Carmichael, 2008), and reducing BC emissions could help to mitigate climate change and improve public health (Jacobson, 2002, 2010; Bond and Sun, 2005).

BC is co-emitted with primary organic aerosol and secondary aerosol precursors such as organic gases and NO_x which, through coagulation and condensation, form an internal mixture that increases BC's cloud nucleation activity (Khalizov et al., 2009) and can amplify light absorption (Schnaiter et al., 2005). The concentric core/shell model is often used to represent the mixing state of BC due to its computational simplicity, and the limited quantitative measurements of particle shape. Within this model, coatings can act as a lens, focusing light onto the absorbing core. This effect has been observed in numerous laboratory studies (Schnaiter et al., 2005; Zhang et al., 2008; Cross et al., 2010; Shiraiwa et al., 2010), but ambient measurements have shown mixed results. Lack et al. (2012) observed a mean enhancement of ~ 40 % in biomass burning emissions, but Cappa et al. (2012) (and subsequently Cappa et al., 2013) observed much smaller enhancements off the Californian coast. Measurements like these rely on the use of thermodenuders to remove all non-BC material, however these instruments are unable to remove refractory coatings such as salts, metals or some organics (Cappa et al., 2013), and nonrefractory aerosol may recondense after the heated section (Fuentes and McFiggans, 2012).

Even when taking into account the limitations of thermodenuders, Cappa et al.'s calculated absorption enhancements exceeded their measurements. Comparisons to detailed optical models (which use more complex soot morphologies) show that the concentric core/shell model overestimates the absorption enhancement due to coatings

AMTD
7, 5491–5532, 2014

(Adachi et al., 2010). However, these models also often show that the absorption of the core is underestimated when assumed to be spherical, as the core's centre is shielded by its edge (Liu et al., 2008; Kahnert et al., 2012). Absorption of a spherical core is also strongly sensitive to the core size distribution, which varies significantly between different BC sources (Huang et al., 2011; Kondo et al., 2011a; Sahu et al., 2012). Finally, absorption of BC in any morphology also depends on the assumed refractive index (Bond and Bergstrom, 2006). When taking into account all these effects, some of which oppose each other, there is little experimental evidence that the concentric core/shell model systematically over- or under-estimates absorption compared to more complex models, as the comparison depends on the properties (either measured or assumed) of the particles in question.

State of the art climate models (e.g. Matsui et al., 2013) use 2-dimensional matrices of particle diameter and BC mass fraction to represent the wide variety of sizes and mixing states of ambient particles. Within the core/shell model, these are analogous to distributions of core size and coating thickness. The Single Particle Soot Photometer (SP2, Droplet Measurement Technologies, Boulder, CO, USA) has emerged as a technique for measuring the distributions of both cores and coatings. The SP2 quantifies refractory black carbon (rBC) mass on a single-particle basis, irrespective of coatings (Moteki and Kondo, 2007; Slowik et al., 2007). This data can then be used to generate distributions of rBC core diameter (D_C). The SP2 is also capable of measuring the scattering cross section of BC-containing particles before they evaporate in the laser beam which, when combined with a Mie core/shell scattering model, can be used to calculate the spherical-equivalent diameter of the whole particle (D_P) (Gao et al., 2007; Moteki and Kondo, 2008). This can then be used to calculate optical properties (Gao et al., 2008; Schwarz et al., 2008b; Shiraiwa et al., 2008). Moteki et al. (2008) (and subsequently Kondo et al., 2011b) described a technique where coating properties were determined by comparing light scattering of the coated particle to that of the core, though this is not used here. Here, we consider the more widely-used technique where coating properties are calculated using the scattering of the coated particle and the

AMTD
7, 5491–5532, 2014

incandescence of the core (Gao et al., 2007). In literature, a range of different assumed rBC densities (ρ_C) and refractive indices (n_C) have been used with this technique.

In this paper, we quantitatively evaluate the capability of the SP2 to determine mixing state using the incandescence/scattering technique, providing a sensitivity analysis of the derived coatings to the assumed density and refractive index of the core. We do not assess the ability of the core/shell model to accurately predict optical properties when using the derived core and coating distributions, as this will be discussed in a future manuscript (Taylor et al., 2014).

2 Experimental setup

2.1 The Pasadena supersite

CalNex-LA, part of the wider CalNex project, took place from 15 May–15 June 2010. The Pasadena supersite has previously been described in detail (Washenfelder et al., 2011; Hayes et al., 2013). Briefly, a wide array of aerosol and gas-phase instrumentation was deployed on the Caltech campus, Pasadena, CA. Atmospheric composition at the site showed a strong weekday diurnal cycle. During the afternoon, an advected plume from the source-rich western LA basin reached the site after around 3 h processing (Washenfelder et al., 2011). At other times, composition at the site was generally representative of fresher, more local emissions, which are found throughout the basin (Metcalf et al., 2012). Non-refractory aerosol composition was typical of a polluted, oxidizing urban environment, with secondary organics dominating during daylight hours, and strong nocturnal ammonium nitrate formation (Hayes et al., 2013). The main source of BC in the region is thought to be diesel emissions, and biomass burning did not strongly influence the site during the measurement period (Bahreini et al., 2012; Hayes et al., 2013).

The site was periodically impacted by emissions from a nearby loading area, specifically those from a large, diesel-powered forklift truck. This was manifested as short but

AMTD
7, 5491–5532, 2014

strong spikes in the SP2 time series and, as these were not deemed representative of the ambient aerosol, these were removed from the dataset.

2.2 Overview of sampling system

The BC instruments consisted of an SP2, 3-wavelength PhotoAcoustic Soot Spectrometer (PASS-3, Droplet Measurement Technologies), Aethalometer and a Soot-Particle Aerosol Mass Spectrometer (SP-AMS, Aerodyne Research Inc., Billerica, MA, USA), though only the SP2 and SP-AMS data are considered here. Figure 1 shows the sampling system used by these instruments during CalNex. A shared 10.1 cm inner-diameter NOAA common inlet, of PVC and aluminium construction, was used to sample from 6.9 m a.g.l. A model 8450 air velocity transducer (TSI Incorporated, Shoreview, MN, USA) in the main inlet ensured flow remained laminar.

Air from the stack was sub-sampled 5.6 m down, perpendicular to the main inlet flow, and dried to 35 % relative humidity using a Nafion drier (Perma Pure, Toms River, New Jersey, USA). The counterflow was provided by a compressor connected to a Hankison membrane drier. Super-micron particles were removed using an inline PM_1 cyclone (URG Corporation, Chapel Hill, North Carolina, USA), through a 3 m long copper tube. The SP2, PASS, SP-AMS and Aethalometer were connected to the cyclone output by approximately 5 m of copper tube, as shown in Fig. 1. From 18 May 2010, the SP2, PASS and SP-AMS sampled through a line, alternating every 10 min between an ambient inlet and a line drawn through a thermodenuder (Huffman et al., 2008).

2.3 The single particle soot photometer

The SP2 (Stephens et al., 2003; Schwarz et al., 2010) measures rBC using the principle of light-induced incandescence. Particles are drawn through a high intensity intracavity 1064 nm Nd:YAG laser; rBC-containing particles absorb the infrared laser radiation and are heated to incandescence, emitting visible light. This light is detected on a particle-by-particle basis by two photomultiplier tubes (PMTs) which are optimized

AMTD
7, 5491–5532, 2014

to different wavelength ranges (broadband and narrowband) to give an indication of the incandescence temperature (Schwarz et al., 2010). The amount of light detected is linearly proportional to the mass of black carbon in a particle, regardless of particle coatings or morphology (Moteki and Kondo, 2007; Slowik et al., 2007). The incandescence channels of the SP2 were calibrated using glassy carbon spheres (Type II, Alfa Aesar, Ward Hill, MA, USA) in the manner described by Liu et al. (2010) and McMeeking et al. (2010). Comparison to NOAA's SP2, calibrated with fullerene soot, showed agreement to within 10 %. The SP2 also has two avalanche photodiode (APD) scattering detectors which were calibrated with polystyrene latex spheres (PSLs; Duke Scientific, now Thermo Fisher Scientific, Waltham, MA, USA). Further details of SP2 calibrations are provided in Supplement Sect. A1.

During CalNex, the high-gain broadband detector measured between 0.2–27 fg (67–305 nm mass-equivalent diameter at core density $\rho_C = 1.8\,g\,cm^{-3}$) and the low-gain narrowband 0.6–130 fg (84–520 nm). The rBC mass concentration was corrected for particles outside the SP2's detection range. Further details are provided in Sect. A2 of the supporting material. A comparison to a co-located Sunset OC/EC instrument is also presented in Sect. A3 of the supporting material. The SP2 showed excellent correlation ($R^2 = 0.94$) with the optical EC channel, and good correlation ($R^2 = 0.58$) with the more common thermal EC channel.

2.4 The Soot Particle-Aerosol Mass Spectrometer

The SP-AMS is a modified version of the HR-ToF Aerosol Mass Spectrometer (AMS; Aerodyne Research Inc., Billerica, Massachusetts, USA). The standard AMS utilizes a tungsten vaporizer heated to 600 °C, and hence cannot measure refractory species which remain solid at this temperature. The SP-AMS uses the same kind of 1064 nm Nd:YAG laser as in the SP2 to selectively vaporize BC-containing particles and measure the composition of core and coating (Onasch et al., 2012). During CalNex, the tungsten vaporizer was removed and only BC-containing particles were vaporized. Note here that we are using the convention of referring to the BC material detected

AMTD
7, 5491–5532, 2014

by the SP-AMS as rBC as recommended by Petzold et al. (2013), though it is not possible to unambiguously determine whether this is equivalent to the material detected by the SP2.

Mass concentrations were calculated using the standard fragmentation table technique (Allan et al., 2004), modified to account for rBC peaks at the m/z channels at multiples of 12, using a rBC relative ionization efficiency of 0.2 (Onasch et al., 2012). Where there was a conflict with other anticipated fragments (e.g. C_3^+ and HCl^+ at $m/z = 36$ and C_4^+ and SO^+ at $m/z = 48$), high resolution analysis (DeCarlo et al., 2006) was employed to determine the fraction as a function of time. While there were theoretically many contributions possible, the high resolution analysis showed that the overwhelming majority of ambient rBC mass was accounted for by the C_1–C_4 fragments.

When attempting to quantify overall mass loadings, poor correlations were found when comparing the SP-AMS with the SP2 and Sunset instrument, in contrast to the measurements of Cappa et al. (2012). Upon investigation, it was found that the quantitative sensitivity of the SP-AMS to rBC was not independent of the other components. A greater fraction of the rBC was detected during periods of high concentrations of inorganics, which is speculatively linked to an improvement of the focusing of the particle beam with larger particles. This comparison is presented in Sect. A3.3 of the Supplement.

Because of this issue, it is not possible to treat the mass concentrations generated by the SP-AMS as absolute, however the relative concentrations reported should be accurate for those particles detected. This is not necessarily representative of the BC-containing particles overall, as the smaller particles that escape detection are likely to have a higher rBC to coating mass ratio. The concentrations of coating materials relative to each other is likely to be more accurate, but it is likely to biased slightly towards secondary rather than primary coatings, as the latter will again be prevalent on the missed particles and be almost purely organic as opposed to mixed organic and inorganic. For the purposes of estimating the shell refractive index (n_S), the reported mass

AMTD
7, 5491–5532, 2014

fractions are used. While it is recognised that this is more likely to be representative of the accumulation mode particles, there is no way of resolving this bias with these data.

2.5 Thermodenuder and data averaging

Semi-volatile aerosol was removed from the sample using a thermodenuder (Aerodyne Research Inc.) (Huffman et al., 2008). Particles were drawn through a heated tube, and vapors were adsorbed onto a charcoal trap. The temperature was cycled on a sawtooth profile, heating from 56–230 °C over 2 h, with a 35 min cool-down period. Temperature was measured using three temperature probes; data were excluded when the standard deviation of the three measurements was > 4 °C, to reduce ambiguity in the internal temperature.

The SP2, PASS and SP-AMS were switched between the thermodenuder and ambient inlet every 10 min, with a bypass flow running through the unused line in order to maintain the temperature profile in the denuder and remove the need to flush out stagnant air after changes. The SP2 data were averaged to a 5 min time basis. Using the 1 s data, a 20 s delay time was observed between the valves switching and the sample line flushing through. Hence, data from the first 20 s of each 5 min period were excluded.

Losses through the thermodenuder were characterized by comparing the ratio of SP2 rBC mass and number concentrations to the average of the adjacent undenuded data points. Transmission of particles through the denuder exhibited a linear relationship with the thermodenuder temperature, parameterized by

$$\text{Transmission} = 0.728 - 0.0006 \times T_{\text{TD}}, \quad (1)$$

where T_{TD} is the average of the thermodenuder's three temperature probes, measured in °C.

Though the slope is similar to that found by Huffman et al. (2008), the intercept is much less than 1, which is likely to be due to the use of a longer charcoal trap after

AMTD
7, 5491–5532, 2014

the denuder. Number and mass losses measured by the SP2 were identical within 2 % across the whole temperature range, suggesting any size-dependence was negligible.

rBC and coating composition through the thermodenuder is presented in Supplement Sect. A4. Though there were still some residual coatings, and the variable collection efficiency of the SP-AMS complicated factors, the majority of coating mass was removed when the thermodenuder was at its highest temperatures.

2.6 Co-located NO, NO_2 and NO_y

NO, NO_2 and NO_y were measured by chemiluminescence using Model 42C-TL detectors (Thermo Fisher Scientific) for NO and NO_y, and model 42i-TL for NO_2. The NO_2 instrument was modified to use a blue LED instead of a molybdenum catalyst to convert NO_2 to NO, to exclude conversion of HNO_3 and PANs (Lefer et al., 2010). The NO_y instrument was used as described by Luke et al. (2010), except the molybdenum catalyst was only heated to 320 °C to reduce possible interference from NH_3 conversion. Data were reported as 1 min averages, and NO_2 data were only available after 17:15 on 27 May. NO_x is calculated as the sum of NO and NO_2. We calculate $-\log(NO_x/NO_y)$ as a qualitative measure of photochemical age (Kleinman et al., 2007), the method also used by Cappa et al. (2012). Data are only considered from periods when all three measurements (NO, NO_2 and NO_y) were available.

3 Calculating rBC coating thickness

In the following section, we describe the data analysis routines and techniques required to use raw SP2 data to calculate coating and optical properties. Whilst the basic technique has been used before (Gao et al., 2007), here we explore the sensitivities of the Mie model to assumptions of density and refractive index, and describe data quality assurance techniques that are necessary for comparison with measured optical

AMTD
7, 5491–5532, 2014

properties. The data presented here were taken after 26 May 2010, when the SP2's detectors were re-aligned.

3.1 The use of the core/shell model

Fresh soot particles often assume the form of fractal aggregates of BC spherules. Over time, mixing with other material by condensation and coagulation causes voids within the aggregates to be filled and the fractal shape to collapse to form a quasi-spherical particle (Zhang et al., 2008; Ghazi and Olfert, 2013). Given the variations in soot morphology, there is question as to the representativeness of the core/shell model, and to the use of scattering to derive coating properties.

Adachi et al. (2013) measured the shapes of soot particles in Pasadena during the same measurement period as this study. While they observed a variety of morphologies and with variable mixing of material, heavily compacted (but uncoated) BC was seen in period of high CO_2 concentrations, which correspond with the processed Western-LA plume reaching the site (Hayes et al., 2013). The dominant aerosol in these plumes was semi-volatile SOA, which Adachi et al. (2013) note they would be unable to detect as it would evaporate before or during the measurement process. Surface tension forces during condensation of coating material is thought to be the process by which fractal soot is compacted, so it therefore seems likely that these particles were coated by SOA that Adachi et al. were unable to detect.

How appropriate the use of light scattering is to derive coating properties depends on the particles in question. Particles small compared to the wavelength of light lie in the Rayleigh regime, where light scattering is independent of particle morphology. For a wavelength of 1064 nm used in the SP2, this regime is appropriate for externally-mixed BC (i.e. with a single refractive index) $< 10^{-20}$ m^3 in volume (equivalent to 267 nm diameter) (Moteki et al., 2010).

For thickly coated particles (which are quasi-spherical in shape due to compaction of the primary BC and filling in voids between spherules), laboratory measurements have shown this method may be used to accurately determine the size of the coated

AMTD
7, 5491–5532, 2014

particle (Shiraiwa et al., 2010). Laborde et al. (2013) also verified accurate sizing using this method for ambient particles with < 35 % rBC volume fraction when compared to particle mobility diameter.

For intermediate coatings, which may not exhibit a core shell morphology, the derived coating thickness is a useful qualitative indicator of mixing state that is widely used. Consideration of the scattering enhancement (compared to an uncoated particle) in any way more complex than a simple coating thickness would require detailed knowledge of particle morphology, measurements of which are extremely limited in terms of time resolution and their ability to measure semi-volatile coatings. Where soot of variable morphology is present (as is almost always the case in ambient environments), particle morphology would also need to be known on a single-particle basis as the particles were measured in the SP2.

Coating thicknesses derived using this technique are therefore considered semi-quantitative in ambient environments. However, in order to be able to interpret these measurements, one needs to be able to accurately predict the amount of light scattered by externally-mixed rBC. Any enhancement of this would then indicate particles are mixed with some amount of nonrefractory material. When using the SP2's incandescence measurement to calculate the core size, the amount of light scattered then depends on the assumed refractive index and density of the core, as well as the calibration of the incandescence detectors. One must also carefully consider the limited detection range of the instrument (both its scattering and incandescence measurements) to avoid bias.

3.2 Overview of technique

For each particle, the incandescence signals are used to calculate the rBC mass, and the scattering signals provide the scattering cross section of the coated particle at 1064 nm, using the signals collected during the period between the particle beginning to interact with the laser beam and the point at which the particle starts to evaporate in the laser.

AMTD
7, 5491–5532, 2014

In order to calculate core and shell diameters, a number of parameters are required. The refractive index of the coating was calculated using the chemical composition of the coating material measured by the SP-AMS and allowed to vary during the course of the campaign. A number of lookup tables were generated for a range of different core and coating refractive indices, and thermally denuded data was used to constrain the most appropriate core density and refractive index, such that the measured scattering matched the modelled scattering if the cores were assumed to be uncoated. Size-dependent factors, such as small signals below detection limit or large signals saturating the detectors, could cause some of the scattering data to be considered unreliable. By examining the size dependence of these factors, a range of core diameters for which the scattering data was considered reliable was identified. Particles from this range were then used to calculate coating thicknesses.

3.3 Determination of optical particle size using the SP2

The SP2 uses two light scattering channels for optical sizing. When the laser and detectors are properly aligned, each purely-scattering particle records a Gaussian profile as it crosses the laser, with magnitude proportional to the laser intensity and scattering cross-section of the particle. For BC-containing particles, material evaporates as they pass through the laser, causing the scattering cross-section to decrease to zero. In order to properly size these particles, leading-edge only (LEO) fitting is used (Gao et al., 2007); the signal as the particles enter the edge of the laser, before material has evaporated, is used to reconstruct the Gaussian profile of the original particle, had it not evaporated. A twin-element avalanche photodiode (TEAPD) was used to constrain the fits, such that the scattered light of the particle moves from one element of the detector to the other as it passes through the laser. The signal on one side is inverted, producing a clear notch as the particle passes the center of the detector and the signal switches from negative to positive. The difference in position between the notch and the peak laser power is fixed during measurements, meaning the position of a BC-containing particle within the beam profile can be inferred to constrain the Gaussian fit

AMTD
7, 5491–5532, 2014

as the Gaussian response of non-absorbing particles is directly measured. For further explanation, the reader should refer to Laborde et al. (2012), where this scheme is presented graphically.

For each LEO fit, the baseline is calculated using the mean of the first six data points (1.2 µs). This is subtracted from the data, and a Gaussian function is then fit to the leading edge data. The modal notch position and width of the previous 200 unsaturated purely-scattering particles are used to constrain the fit, leaving the fit amplitude as the only free parameter. We define the leading edge as all data from the baseline-subtracted zero up to 5 % of the maximum laser intensity, with the x position calculated using the fit position and width assuming a Gaussian laser profile. This was determined by examining the time-dependent scattering cross section for incandescent particles (Moteki and Kondo, 2008; Laborde et al., 2012).

A large fraction of particles evaporated before the notch position could be properly determined. Rather than rising above the baseline as the particle passes across the split in the TEAPD, these particles' signals merely fell back to the baseline, giving no indication of position within the laser. To remove this ambiguity, in this dataset we redefine the notch position based on the point where the scattering signal crosses 20 mV × 2.44 mV units above the baseline rather than the baseline itself, such that particles that evaporate before the split are not counted for the purposes of particle size measurements. Note that the incandescence signal is still reported for these particles, so this does not affect the rBC mass concentrations reported.

Gao et al. (2007) identified particles with scattering signals too small to reliably size, as they generate noisy fits, and those with large signals that saturated the scatter detector within the leading edge, as unreliable fits. Schwarz et al. (2008b) explored the effect of assuming the thinnest and thickest possible coatings for these particles, and reported coating properties as the average of these two extremes. In this analysis we avoid this issue by choosing the core diameter range in which particle coatings are considered such that these particles only make up a small fraction of particles, and do not affect derived coating properties. This is discussed more fully in the next section.

AMTD
7, 5491–5532, 2014

A series of filters was also used to identify and discard LEO fits that were poor due to electronic noise or coincident particles, though this affected < 0.01 % of incandescence triggers.

3.4 Determining a core size range for unbiased coating analysis

In order to minimize bias in the results, it is necessary to examine the distribution of detectable notch position and good LEO fits vs. an independent variable, in this case core diameter. The range of these parameters varies depending on the instrumental setup of the SP2.

Figure 2a shows the fraction of particles with detectable notch position (F_{Notch}) as a function of D_C. The smallest cores, $D_C < 100$ nm, show approximately 10 % detectable notch position, as most particles in this size range do not scatter enough light to be detected on either scatter detector. The ambient particles show a higher F_{Notch} than the denuded, as the ambient particles are, on average, more coated, and so a greater fraction of the smaller particles can be detected.

Figure 2b–e examine the probability distribution function of E_{Sca}, the ratio of a particle's measured scattering cross section divided by that of its uncoated core predicted by Mie theory, integrated over the detection angles of the SP2. Figure 2b shows how $dP/d\log(E_{Sca})$ varies with core diameter for the cases most influenced by fresh emissions. These are defined as particles which have passed through the thermodenuder set at a temperature of greater than 220 °C, during periods when ambient $-\log(NO_x/NO_y)$ was lowest (defined as being less than 0.08, the 10th percentile). These particles are the least chemically aged, and have had almost all of their coatings removed by the thermodenuder. Such particles with a D_C less than 100 nm show E_{Sca} values greater than one, as only the most coated particles are detected. Using data from this range of core diameter would result in a bias towards thickly coated particles.

At core diameters 100–135 nm, F_{Notch} increases and the distribution of E_{Sca} shifts closer to one as the bulk of BC-containing particles become detectable in both scatter

AMTD
7, 5491–5532, 2014

detectors. At D_C = 135 nm the two traces on Fig. 2a converge, and therefore F_{Notch} is independent of coatings. This is also the point where F_{Notch} reaches 50 %. We choose this as the lower bound of the region in which to consider LEO fitting.

Figure 2c shows $dP/d\log(E_{Sca})$ vs. core diameter of particles sampled under the most processed conditions. Such conditions are defined as being when particles are sampled through the ambient inlet and the ambient $-\log(NO_x/NO_y)$ was greater than 0.34 (the 90th percentile). The upper edge of the E_{Sca} distribution is limited by saturation of the low-gain scatter detector. It is clear that for large core sizes, a significant fraction of the most coated particles are limited by saturation. We choose D_C = 200 nm as the upper bound of the region in which coatings are considered, in order to limit this bias affecting the data.

Although there is some user input in determining the D_C limits, we have detailed a logical method to determine reasonable values. For comparison, shifting the limits by 5 nm either way (i.e. $130 \le D_C \le 195$ and $140 \le D_C \le 205$) affected campaign-average coatings by < 1 %.

Figure 2d and e show $dP/d\log(E_{Sca})$ for $135 \le D_C \le 200$ nm for the least coated and most coated particles respectively. Whilst this does not cover the entire rBC mass distribution, it is likely representative of the majority of ambient absorbing aerosol. For our choice of density and refractive index (discussed in Sect. 3.6) the least coated particles show E_{Sca} has a modal value close to 1, signifying uncoated particles, and for the most coated particles there is a clear shift towards larger E_{Sca}.

To summarize, scattering measurements on particles with the smallest core size detected by the SP2 are biased towards the most coated particles, whilst particles with the largest cores are biased towards the least coated. These are due to scattering signals being below the detection limit, or above the saturation level, of the scattering detectors. This section has outlined a method to choose a range of core diameters that are least affected by these problems, to gain the most representative results possible.

AMTD
7, 5491–5532, 2014

3.5 The Mie model

A scattering model is used to relate the measured scattering signal to particle diameter (Gao et al., 2007). For BC-containing particles, we assume a concentric sphere core-shell configuration, and use Mie theory to calculate the scattering cross-sections. We used Scattnlay Mie code (Pena and Pal, 2009), which uses the same equations developed by Yang (2003) but runs in C. For ease of use and computational efficiency, this was compiled as an external operation (XOP) for Igor Pro (Wavemetrics, Portland, OR, USA).

A series of 2-dimensional lookup tables were produced containing scattering cross-sections for $\lambda = 1064$ nm, integrated over the angles of the SP2's APDs (Moteki and Kondo, 2007), for core diameter $80 \leq D_C \leq 600$ nm and coated diameter $100 \leq D_P \leq 600$ nm, with 1 nm resolution. 600 nm is considered the upper limit, as we were unable to reliably sample calibration particles larger than this size. Different tables must be used for different core and shell refractive indices. For each particle, D_C is calculated using the incandescence data as described in Sect. 2.3 and D_P is then interpolated using the selected look-up table, normalized to the measured scattering signal of a 200 nm PSL. The most basic product of Mie theory in the context of the SP2 is E_{Sca}, the enhancement in a particle's scattering cross section (integrated over the angles of the SP2's scatter detectors) compared to that of its uncoated core. To calculate this, only the rBC core density and refractive index are necessary, whereas calculating a coating thickness also requires the refractive index of the coating. Some particles recorded $E_{Sca} < 1$, such that the LEO scattering signal is smaller than Mie theory predicts for an uncoated core. This is equivalent to a negative coating thickness, which is nonphysical. These measurements are partly a consequence of random errors associated with the LEO fitting, but their likelihood is also strongly affected by the core density and refractive index used (this is discussed in the next section). In order to include these particles in coating calculations, they are assigned a coating thickness of zero. This approach does not affect the median shell/core ratio, though it may slightly

AMTD
7, 5491–5532, 2014

bias any calculated bulk optical properties towards more coated particles. Discarding these particles would bias the data even further, as only the thickest coatings would be counted.

3.6 Sensitivity to density and refractive index

As noted in the previous section, calculation of E_{Sca} requires prior knowledge of the density and complex refractive index of the rBC core. Using a higher refractive (real and imaginary) index increases the scattering efficiency of the rBC core, and consequently reduces the calculated E_{Sca}. Conversely, the scattering cross section of a particle of given mass scales approximately with $\rho_C^{2/3}$, so increasing density increases E_{Sca}. These two parameters have been the subject of a large body of previous research, extensively reviewed by Bond and Bergstrom (2006). They recommended densities between $1.7 \le \rho_C \le 1.9\,g\,cm^{-3}$ and refractive indices in the range $(1.75 - 0.63i) \le n_C \le (1.95 - 0.79i)$, noting the higher refractive (real and imaginary) indices looked the most promising. More recently, Moteki et al. (2010) used SP2 LEO measurements to infer $n_C = (2.26 - 1.26i)$ for denuded ambient soot in Tokyo, assuming a density $\rho_C = 1.8\,g\,cm^{-3}$. These parameters were recently used by Laborde et al. (2013) to explore the properties of rBC in Paris. A variety of other parameters have been used in previous publications. These are discussed in Sect. A5 of the Supplement, and summarized in Table 1.

Figure 3 demonstrates the sensitivity of calculated scattering cross section of uncoated rBC cores to density and refractive index, using the parameters in Table 1. While there appears to be a central group of similar cross sections, the difference between the highest and the lowest is a factor of 3. This equates to a difference in a factor of 3 when calculating E_{Sca}, and hence a significant change in calculated coating thickness. The effect this has on the measured distribution of E_{Sca} is shown in Fig. 4a for particles measured during the same least-processed conditions as presented in Fig. 2. The spread in the data is due to a combination of random error in the LEO fits,

AMTD
7, 5491–5532, 2014

particles passing through different parts of the laser, and some remaining coatings on the particles at 220 °C. Ideally the distribution should be centred around 1 for uncoated particles. The fraction of particles with $E_{Sca} < 1$ is strongly dependent on the core refractive index and density used, as would be the bias associated with discarding these particles for coating calculations.

It is encouraging that the density and refractive index recommended by Moteki et al. (2010), measured by a similar technique, result in a distribution centred close to 1. Moteki et al. (2010) conducted their measurements at 1064 nm, whereas the others were either for visible wavelengths or broadband spectra. We therefore consider the parameters derived by Moteki et al. (2010) the most appropriate to use for this dataset, and likely other SP2 measurements where diesel engines are the dominant source of black carbon. Under the assumption that they represent the closest estimate to the physical properties of the measured rBC, all other parameters lead to an overestimation of E_{Sca}, and further analysis would therefore overestimate coating thickness and absorption enhancement, for a given coating refractive index.

Figure 4b and c explore the sensitivity of the E_{Sca} distribution to density and refractive index seperately. It is clear that within the range of parameters used, there is greater sensitivity to refractive index than density.

3.7 Calculating the coating refractive index using the SP-AMS

In order to convert E_{Sca} into a physical coating thickness, as described in Sect. 3.4, a coating refractive index must be assumed, in addition to the core density and refractive index. Previous studies have assumed a constant value, generally close to 1.5. We instead used the relative contributions of organics, nitrate, and sulphate measured by the SP-AMS to calculate a time-dependent refractive index using volume mixing rules (Stelson, 1990). Nitrate and sulphate were assumed to be associated with ammonium cations as the aerosol in Pasadena was for the most part neutralized (Hayes et al., 2013). Inorganic densities were taken from Weast (1977), and the density of organics was assumed to be 1.2 g cm^{-3}, as suggested by Stelson (1990). This yields a refractive

AMTD
7, 5491–5532, 2014

index of organics of 1.46, which is in the range typically assumed for organics, though it has been shown that oxidation of organics can increase both density (Kroll et al., 2009) and refractive index. Cappa et al. (2011), with opposing effects on scattering calculations. The mean refractive index for the ambient data calculated with this approach is 1.48 ± 0.01 (one standard deviation). This number is dominated by organics, which form the bulk of the coating (we discuss this further in Taylor et al., 2014). Changes were due to variation in the organic/inorganic fractions in ambient aerosol, and clear differences were observed when switching to the thermodenuder.

3.8 Sources of uncertainty

Uncertainties associated with the derivation of coating thicknesses have been discussed previously (Gao et al., 2007; Schwarz et al., 2008b). Some sources are relatively simple to quantify. The main source of statistical uncertainty is the position of a particle in the laser beam, which affects the amount of scattered light as well as the FWHM and notch position (while the notch position measures a particle's passage through the laser in terms of time it does not measure how close a particle passes to the laser's peak intensity at the centre of the beam). Calibrations with 200 nm PSLs showed the error on the full Gaussian fit was ~ 30 %, but increased to 50 % when using LEO fits (up to 5 % of peak laser power) due to the decreased signal. For comparability, the amount of light scattered by a 200 nm PSL is similar to that scattered by a 149 nm rBC core when using a refractive index of $n_C = (2.26 - 1.26i)$. After the TEAPD was realigned on 26 May, the modal signal of 200 nm PSL calibrations throughout the campaign were all within 3 %, demonstrating the stability of the laser power and scattering detectors. As discussed in Supplement Sect. A1, the single-particle statistical uncertainty in incandescence signal is ~ 30 %, but overall accuracy in D_C is ~ 3 %.

Some uncertainties are difficult to investigate, but thought to be relatively small. The FWHM and notch position are constant for small particles, but for larger ones show some variation as these particles take longer to traverse the laser beam. However, 200 nm and 300 nm PSLs show similar distributions of FWHM and notch position,

AMTD
7, 5491–5532, 2014

meaning for particles < 300 nm in total diameter (which represent the vast majority of rBC number) this sensitivity is small. The fraction of peak laser power used to generate the LEO fits could be a sensitivity, however Laborde et al. (2012) demonstrated the scattering cross-section of coated particles is stable before they start to evaporate in the laser. As discussed in Sect. 3.3, inspection of single particles showed that 5 % of the peak laser power was within this plateau.

As discussed in Sect. 3.1, scattering at 1064 nm is not thought to be sensitive to particle shape for the sizes of externally-mixed particles considered here. For coated rBC shape may affect scattered light but, as we have already discussed, when soot is not in a core/shell configuration the derived coating thicknesses are only a qualitative indicator of mixing state.

For the purposes of this work it is most important to work out the overall uncertainty, not diagnose different sources of it. For the distributions of E_{Sca} shown in Fig. 4, the spread of the distribution is ~ 85 %. Each of these distributions represents the average of ~ 15 000 particles. The precision of the derived coating thicknesses is discussed in the next section.

4 The effect of core density and refractive index on derived coating thickness and absorption enhancement

Using the coating refractive index calculated from the SP-AMS, the absolute and relative coating thicknesses of BC-containing particles were calculated for particles with rBC core diameter in the range discussed previously. Figure 5 shows the distributions of coating thickness under the same conditions as Fig. 4, using the combinations of core density and refractive index that resulted in the smallest and largest E_{Sca}. Gaussian fits to the distributions yield the accuracy and precision of using this technique to determine whether BC-containing particles are externally mixed. Using a core density $\rho_C = 1.8\,g\,cm^{-3}$ and refractive index $n_C = (2.26 - 1.26i)$ generates a distribution of shell/core ratio of 1.04 ± 0.21, corresponding to an absolute coating thickness

AMTD
7, 5491–5532, 2014

distribution of 1.7 ± 17.5 nm. For comparison, a density $\rho_C = 2\,g\,cm^{-3}$ and refractive index $n_C = (1.76 - 0.44i)$ generates a distribution of shell/core ratio of 1.40 ± 0.19, corresponding to an absolute coating thickness distribution of 30.3 ± 14.9 nm.

This demonstrates that when using the right parameters, this technique can accurately determine the mixing state (externally vs. internally mixed) of ambient BC-containing particles, but with limited precision. We note however that the precision will depend on the specific setup of the instrument (e.g. alignment, detector gain settings). If used with different parameters, the precision is similar but accuracy is not guaranteed with ambient soot.

Figure 6 shows the effect these systematic offsets have on the measured shell/core ratios over the whole campaign. Using the density and refractive index recommended by Moteki et al. (2010), and shown in Sect. 3.6 to be the most appropriate for this dataset, results in the lowest coating thicknesses. A hypothetical comparison between parallel analyses using these parameters, and any one of the others used, could result in the conclusion that one set of particles were significantly more coated than the other, when in fact they were identical. This must therefore be considered when comparing datasets using this technique.

While the use of different core density and refractive index may artificially cause a systematic offset in reported coating parameters, there is also variation due to real changes in the ambient particles. Figure 7 compares changes in the median shell/core ratio, again using the refractive index and density combinations that result in the thickest and thinnest coatings, as a function of photochemical ageing. Changes in coatings are captured regardless of the parameters used, but there is a significant offset between the data using the different sets of density and refractive index of the rBC core. The range of coating thicknesses reported does have a dependence on these parameters, but this is small compared to the difference in the absolute values.

Coatings were thickest in the most processed airmasses, similar to results reported from urban plumes in the western Pacific, (Moteki et al., 2007; Shiraiwa et al., 2007) and in California, including some in the Los Angeles area (Sahu et al., 2012). It is

AMTD
7, 5491–5532, 2014

difficult to directly compare coating thicknesses between these studies, due to the different coating metrics and rBC core size ranges used, and the differences shown in Fig. 4. What is consistent between these studies is that, in regions where secondary aerosols also constitute a large fraction of submicron particulate matter, condensation of secondary material increases BC coatings with age. Even using the core parameters that result in the thinnest coatings, the freshest ambient BC-containing particles were also associated with some coating material.

Coatings measured through the thermodenuder were thinner than ambient coatings, though this difference was smallest in the least processed airmasses as the ambient particles were less coated. When using the core parameters that result in the thickest coatings, even the thermodenuded particles appear to have significant coating material. Taking these data in isolation could therefore lead to misleading conclusions about BC's optical properties and cloud condensation nuclei (CCN) activity. This must be considered if SP2 coating data generated in this way are to be used quantitatively.

5 Conclusions

We have demonstrated that optical properties derived by core/shell modelling of SP2 data show a strong sensitivity to assumed rBC core refractive index and density. For a given measured scattering signal and core mass, a larger refractive index (real and imaginary) and smaller core density result in a larger scattering cross section due to the core, meaning less is attributed to a coating. This results in thinner calculated coating thicknesses for the same measured data.

An assessment of the coating properties of freshly-emitted, thermodenuded ambient particles demonstrated that, when using the appropriate core density and refractive index, the SP2 incandescence/scattering technique can accurately determine the mixing state (externally or internally mixed) of ambient rBC. Using a core density $\rho_C = 1.8\,\mathrm{g\,cm^{-3}}$ (Bond and Bergstrom, 2006) and refractive index $n_C = (2.26 - 1.26i)$

AMTD
7, 5491–5532, 2014

(Moteki et al., 2010) generated a distribution of shell/core ratio of 1.04 ± 0.21, corresponding to an absolute coating thickness distribution of 1.7 ± 17.5 nm.

When other core parameters were used, this caused a systematic offset in the reported coating data. Using the core parameters that resulted in the thickest coatings (on the same particles as before) generated a distribution of shell/core ratio of 1.40 ± 0.19, corresponding to an absolute coating thickness distribution of 30.3 ± 14.9 nm. The precision of these measurements will depend on the instrumental setup of the SP2, and the new 8-channel instrument may represent an improvement on these values.

Temporal changes in coating thickness were also measured, and coatings were thickest in the most processed airmasses. This is similar to previous results from California and the western Pacific, where a large fraction of submicron aerosol is also secondary, and suggests a consistent picture of increase coating by condensation of secondary aerosol. While these changes in coating thickness were captured well regardless of the density and refractive input into the Mie model, the sensitivity to assumed core properties must be taken into account when comparing different datasets, or using SP2 coating data to feed into climate models. Omitting this information could lead to misleading conclusions regarding BC's optical properties and CCN activity.

It was not in the scope of this manuscript to assess the appropriateness of the concentric core/shell model to predict bulk optical properties, which detailed optical models report may (or may not) under- or over-predict absorption depending on the particles in question and the wavelength. Comparison of optical properties using this technique will be presented in a future manuscript (Taylor et al., 2014).

The Supplement related to this article is available online at doi:10.5194/amtd-7-5491-2014-supplement.

Acknowledgements. The authors thank J. Jimenez, J. Stutz, J. de Gouw and J. Seinfeld for co-organizing the CalNex-LA site in Pasadena, and the California Air Resources Board and California Institute of Technology for providing funding and logistic support for the ground-site.

AMTD
7, 5491–5532, 2014

We thank K. Froyd, S. M. Murphy and D. Murphy for the setup and use of their sampling inlet and DMA, J. Smith for the loan of the thermodenuder and P. Chhabra for logistical support. We thank P. Zeiger, M. Gysel and J. Crosier for their technical assistance in generating the Mie look-up tables, and J. Schwarz and A. Perring for useful discussions. The University of Manchester activities were supported by The UK Natural Environment Research Council through a PhD studentship and the project Multiscale Chemical Composition of Carbonaceous particles and Coatings (MC4) [Grant ref: NE/H008136/1].

References

Adachi, K. and Buseck, P. R.: Changes of ns-soot mixing states and shapes in an urban area during CalNex, J. Geophys. Res.-Atmos., 118, 3723–3730, doi:10.1002/jgrd.50321, 2013.

Adachi, K., Chung, S. H., and Buseck, P. R. C.-D.: Shapes of soot aerosol particles and implications for their effects on climate, J. Geophys. Res., 115, D15206, doi:10.1029/2009jd012868, 2010.

Allan, J. D., Delia, A. E., Coe, H., Bower, K. N., Alfarra, M. R., Jimenez, J. L., Middlebrook, A. M., Drewnick, F., Onasch, T. B., Canagaratna, M. R., Jayne, J. T., and Worsnop, D. R.: A generalised method for the extraction of chemically resolved mass spectra from Aerodyne aerosol mass spectrometer data, J. Aerosol Sci., 35, 909–922, doi:10.1016/j.jaerosci.2004.02.007, 2004.

Bahreini, R., Middlebrook, A. M., de Gouw, J. A., Warneke, C., Trainer, M., Brock, C. A., Stark, H., Brown, S. S., Dube, W. P., Gilman, J. B., Hall, K., Holloway, J. S., Kuster, W. C., Perring, A. E., Prevot, A. S. H., Schwarz, J. P., Spackman, J. R., Szidat, S., Wagner, N. L., Weber, R. J., Zotter, P., and Parrish, D. D. C.-L.: Gasoline emissions dominate over diesel in formation of secondary organic aerosol mass, Geophys. Res. Lett., 39, L06805, doi:10.1029/2011gl050718, 2012.

Bond, T. C. and Bergstrom, R. W.: Light absorption by carbonaceous particles: an investigative review, Aerosol Sci. Tech., 40, 27–67, doi:10.1080/02786820500421521, 2006.

Bond, T. C. and Sun, H. L.: Can reducing black carbon emissions counteract global warming?, Environ. Sci. Technol., 39, 5921–5926, doi:10.1021/es0480421, 2005.

Bond, T. C., Doherty, S. J., Fahey, D. W., Forster, P. M., Berntsen, T., DeAngelo, B. J., Flanner, M. G., Ghan, S., Kärcher, B., Koch, D., Kinne, S., Kondo, Y., Quinn, P. K., Sarofim, M. C.,

AMTD
7, 5491–5532, 2014

Schultz, M. G., Schulz, M., Venkataraman, C., Zhang, H., Zhang, S., Bellouin, N., Guttikunda, S. K., Hopke, P. K., Jacobson, M. Z., Kaiser, J. W., Klimont, Z., Lohmann, U., Schwarz, J. P., Shindell, D., Storelvmo, T., Warren, S. G., and Zender, C. S.: Bounding the role of black carbon in the climate system: a scientific assessment, J. Geophys. Res.-Atmos., 118, 1–173, doi:10.1002/jgrd.50171, 2013.

Cappa, C. D., Che, D. L., Kessler, S. H., Kroll, J. H., and Wilson, K. R. C.-D.: Variations in organic aerosol optical and hygroscopic properties upon heterogeneous OH oxidation, J. Geophys. Res., 116, D15204, doi:10.1029/2011jd015918, 2011.

Cappa, C. D., Onasch, T. B., Massoli, P., Worsnop, D. R., Bates, T. S., Cross, E. S., Davidovits, P., Hakala, J., Hayden, K. L., Jobson, B. T., Kolesar, K. R., Lack, D. A., Lerner, B. M., Li, S.-M., Mellon, D., Nuaaman, I., Olfert, J. S., Petaja, T., Quinn, P. K., Song, C., Subramanian, R., Williams, E. J., and Zaveri, R. A.: Radiative absorption enhancements due to the mixing state of atmospheric black carbon, Science, 80, 1078–1081 , doi:10.1126/science.1223447, 2012.

Cappa, C. D., Onasch, T. B., Massoli, P., Worsnop, D. R., Bates, T. S., Cross, E. S., Davidovits, P., Hakala, J., Hayden, K. L., Jobson, B. T., Kolesar, K. R., Lack, D. A., Lerner, B. M., Li, S.-M., Mellon, D., Nuaaman, I., Olfert, J. S., Petaja, T., Quinn, P. K., Song, C., Subramanian, R., Williams, E. J., and Zaveri, R. A.: Response to Comment on "Radiative absorption enhancements due to the mixing state of atmospheric black carbon," Science, 80, p. 339, doi:10.1126/science.1230260, 2013.

Cross, E. S., Onasch, T. B., Ahern, A., Wrobel, W., Slowik, J. G., Olfert, J., Lack, D. A., Massoli, P., Cappa, C. D., Schwarz, J. P., Spackman, J. R., Fahey, D. W., Sedlacek, A., Trimborn, A., Jayne, J. T., Freedman, A., Williams, L. R., Ng, N. L., Mazzoleni, C., Dubey, M., Brem, B., Kok, G., Subramanian, R., Freitag, S., Clarke, A., Thornhill, D., Marr, L. C., Kolb, C. E., Worsnop, D. R., and Davidovits, P.: Soot particle studiesinstrument inter-comparisonproject overview, Aerosol Sci. Tech., 44, 592–611, doi:10.1080/02786826.2010.482113, 2010.

DeCarlo, P. F., Kimmel, J. R., Trimborn, A., Northway, M. J., Jayne, J. T., Aiken, A. C., Gonin, M., Fuhrer, K., Horvath, T., Docherty, K. S., Worsnop, D. R., and Jimenez, J. L.: Field-deployable, high-resolution, time-of-flight aerosol mass spectrometer, Anal. Chem., 78, 8281–8289, doi:10.1021/ac061249n, 2006.

AMTD
7, 5491–5532, 2014

Fuentes, E. and McFiggans, G.: A modeling approach to evaluate the uncertainty in estimating the evaporation behaviour and volatility of organic aerosols, Atmos. Meas. Tech., 5, 735–757, doi:10.5194/amt-5-735-2012, 2012.

Gao, R. S., Schwarz, J. P., Kelly, K. K., Fahey, D. W., Watts, L. A., Thompson, T. L., Spackman, J. R., Slowik, J. G., Cross, E. S., Han, J.-H. H., Davidovits, P., Onasch, T. B., and Worsnop, D. R.: A novel method for estimating light-scattering properties of soot aerosols using a modified single-particle soot photometer, Aerosol Sci. Tech., 41, 125–135, doi:10.1080/02786820601118398, 2007.

Gao, R. S., Hall, S. R., Swartz, W. H., Schwarz, J. P., Spackman, J. R., Watts, L. A., Fahey, D. W., Aikin, K. C., Shetter, R. E., and Bui, T. P. C.-D.: Calculations of solar shortwave heating rates due to black carbon and ozone absorption using in situ measurements, J. Geophys. Res., 113, D14203, doi:10.1029/2007jd009358, 2008.

Ghazi, R. and Olfert, J. S.: Coating mass dependence of soot aggregate restructuring due to coatings of oleic acid and dioctyl sebacate, Aerosol Sci. Tech., 47, 192–200, doi:10.1080/02786826.2012.741273, 2013.

Hayes, P. L., Ortega, A. M., Cubison, M. J., Froyd, K. D., Zhao, Y., Cliff, S. S., Hu, W. W., Toohey, D. W., Flynn, J. H., Lefer, B. L., Grossberg, N., Alvarez, S., Rappenglück, B., Taylor, J. W., Allan, J. D., Holloway, J. S., Gilman, J. B., Kuster, W. C., de Gouw, J. A., Massoli, P., Zhang, X., Liu, J., Weber, R. J., Corrigan, A. L., Russell, L. M., Isaacman, G., Worton, D. R., Kreisberg, N. M., Goldstein, A. H., Thalman, R., Waxman, E. M., Volkamer, R., Lin, Y. H., Surratt, J. D., Kleindienst, T. E., Offenberg, J. H., Dusanter, S., Griffith, S., Stevens, P. S., Brioude, J., Angevine, W. M., and Jimenez, J. L.: Organic aerosol composition and sources in Pasadena, California, during the 2010 CalNex campaign, J. Geophys. Res.-Atmos., 118, 9233–9257, doi:10.1002/jgrd.50530, 2013.

Hess, M., Koepke, P., and Schult, I.: Optical properties of aerosols and clouds: the software package OPAC, B. Am. Meteorol. Soc., 79, 831–844, doi:10.1175/1520-0477(1998)079<0831:opoaac>2.0.co;2, 1998.

Huang, X. F., Gao, R. S., Schwarz, J. P., He, L. Y., Fahey, D. W., Watts, L. A., McComiskey, A., Cooper, O. R., Sun, T. L., Zeng, L. W., Hu, M., and Zhang, Y. H.: Black carbon measurements in the Pearl River Delta region of China, J. Geophys. Res., 116, D12208, doi:10.1029/2010jd014933, 2011.

Huffman, J. A., Ziemann, P. J., Jayne, J. T., Worsnop, D. R., and Jimenez, J. L.: Development and characterization of a fast-stepping/scanning thermodenuder for

AMTD
7, 5491–5532, 2014

chemically-resolved aerosol volatility measurements, Aerosol Sci. Tech., 42, 395–407, doi:10.1080/02786820802104981, 2008.
Jacobson, M. Z.: Control of fossil-fuel particulate black carbon and organic matter, possibly the most effective method of slowing global warming, J. Geophys. Res., 107, 4410, doi:10.1029/2001JD001376, 2002.
Jacobson, M. Z.: Short-term effects of controlling fossil-fuel soot, biofuel soot and gases, and methane on climate, Arctic ice, and air pollution health, J. Geophys. Res., 115, D14209, doi:10.1029/2009JD013795, 2010.
Janssen, N. A. H., Gerlofs-Nijland, M. E., Lanki, T., Salonen, R. O., Cassee, F., Hoek, G., Fischer, P., Brunekreef, B., and Krzyzanowski, M.: Health Effects of Black Carbon, edited by: Bohr, R., World Health Organisation, Copenhagen, Denmark, 2012.
Kahnert, M., Nousiainen, T., Lindqvist, H., and Ebert, M.: Optical properties of light absorbing carbon aggregates mixed with sulfate: assessment of different model geometries for climate forcing calculations, Opt. Express, 20, 10042–10058, doi:10.1364/oe.20.010042, 2012.
Khalizov, A. F., Zhang, R., Zhang, D., Xue, H., Pagels, J., and McMurry, P. H.: Formation of highly hygroscopic soot aerosols upon internal mixing with sulfuric acid vapor, J. Geophys. Res., 114, D05208, doi:10.1029/2008JD010595, 2009.
Kleinman, L. I., Daum, P. H., Lee, Y.-N., Senum, G. I., Springston, S. R., Wang, J., Berkowitz, C., Hubbe, J., Zaveri, R. A., Brechtel, F. J., Jayne, J., Onasch, T. B., and Worsnop, D. C.-D.: Aircraft observations of aerosol composition and ageing in New England and Mid-Atlantic States during the summer 2002 New England Air Quality Study field campaign, J. Geophys. Res., 112, D09310, doi:10.1029/2006jd007786, 2007.
Kondo, Y., Matsui, H., Moteki, N., Sahu, L., Takegawa, N., Kajino, M., Zhao, Y., Cubison, M. J., Jimenez, J. L., Vay, S., Diskin, G. S., Anderson, B., Wisthaler, A., Mikoviny, T., Fuelberg, H. E., Blake, D. R., Huey, G., Weinheimer, A. J., Knapp, D. J., and Brune, W. H.: Emissions of black carbon, organic, and inorganic aerosols from biomass burning in North America and Asia in 2008, J. Geophys. Res., 116, D08204, doi:10.1029/2010JD015152, 2011a.
Kondo, Y., Sahu, L., Moteki, N., Khan, F., Takegawa, N., Liu, X., Koike, M., and Miyakawa, T.: Consistency and traceability of black carbon measurements made by laser-induced incandescence, thermal-optical transmittance, and filter-based photo-absorption techniques, Aerosol Sci. Tech., 45, 295–312, doi:10.1080/02786826.2010.533215, 2011b.
Kroll, J. H., Smith, J. D., Che, D. L., Kessler, S. H., Worsnop, D. R., and Wilson, K. R.: Measurement of fragmentation and functionalization pathways in the heterogeneous oxidation of

AMTD
7, 5491–5532, 2014

oxidized organic aerosol, Phys. Chem. Chem. Phys., 11, 8005–8014, doi:10.1039/b905289e, 2009.

Laborde, M., Mertes, P., Zieger, P., Dommen, J., Baltensperger, U., and Gysel, M.: Sensitivity of the Single Particle Soot Photometer to different black carbon types, Atmos. Meas. Tech., 5, 1031–1043, doi:10.5194/amt-5-1031-2012, 2012.

Laborde, M., Crippa, M., Tritscher, T., Jurányi, Z., Decarlo, P. F., Temime-Roussel, B., Marchand, N., Eckhardt, S., Stohl, A., Baltensperger, U., Prévôt, A. S. H., Weingartner, E., and Gysel, M.: Black carbon physical properties and mixing state in the European megacity Paris, Atmos. Chem. Phys., 13, 5831–5856, doi:10.5194/acp-13-5831-2013, 2013.

Lack, D. A., Langridge, J. M., Bahreini, R., Cappa, C. D., Middlebrook, A. M., and Schwarz, J. P.: Brown carbon and internal mixing in biomass burning particles, P. Natl. Acad. Sci. USA, 109, 14802–14807, doi:10.1073/pnas.1206575109, 2012.

Langridge, J. M., Lack, D., Brock, C. A., Bahreini, R., Middlebrook, A. M., Neuman, J. A., Nowak, J. B., Perring, A. E., Schwarz, J. P., Spackman, J. R., Holloway, J. S., Pollack, I. B., Ryerson, T. B., Roberts, J. M., Warneke, C., de Gouw, J. A., Trainer, M. K., and Murphy, D. M. C.-D.: Evolution of aerosol properties impacting visibility and direct climate forcing in an ammonia-rich urban environment, J. Geophys. Res., 117, D00V11, doi:10.1029/2011jd017116, 2012.

Lefer, B., Rappenglueck, B., Flynn, J., and Haman, C.: Photochemical and meteorological relationships during the Texas-II Radical and Aerosol Measurement Project (TRAMP), Atmos. Environ., 44, 4005–4013, doi:10.1016/j.atmosenv.2010.03.011, 2010.

Liu, D., Flynn, M., Gysel, M., Targino, A., Crawford, I., Bower, K., Choularton, T., Jurányi, Z., Steinbacher, M., Hüglin, C., Curtius, J., Kampus, M., Petzold, A., Weingartner, E., Baltensperger, U., and Coe, H.: Single particle characterization of black carbon aerosols at a tropospheric alpine site in Switzerland, Atmos. Chem. Phys., 10, 7389–7407, doi:10.5194/acp-10-7389-2010, 2010.

Liu, L., Mishchenko, M. I., and Arnott, W. P.: A study of radiative properties of fractal soot aggregates using the superposition T-matrix method, J. Quant. Spectrosc. Ra., 109, 2656–2663, doi:10.1016/j.jqsrt.2008.05.001, 2008.

Luke, W. T., Kelley, P., Lefer, B. L., Flynn, J., Rappenglueck, B., Leuchner, M., Dibb, J. E., Ziemba, L. D., Anderson, C. H., and Buhr, M.: Measurements of primary trace gases and NO_y composition in Houston, Texas, Atmos. Environ., 44, 4068–4080, doi:10.1016/j.atmosenv.2009.08.014, 2010.

AMTD
7, 5491–5532, 2014

Marley, N. A., Gaffney, J. S., Baird, C., Blazer, C. A., Drayton, P. J., and Frederick, J. E.: An empirical method for the determination of the complex refractive index of size-fractionated atmospheric aerosols for radiative transfer calculations, Aerosol Sci. Tech., 34, 535–549, doi:10.1080/02786820118599, 2001.

Matsui, H., Koike, M., Kondo, Y., Moteki, N., Fast, J. D., and Zaveri, R. A.: Development and validation of a black carbon mixing state resolved three-dimensional model: aging processes and radiative impact, J. Geophys. Res.-Atmos., 118, 2304–2326, doi:10.1029/2012JD018446, 2013.

McMeeking, G. R., Hamburger, T., Liu, D., Flynn, M., Morgan, W. T., Northway, M., Highwood, E. J., Krejci, R., Allan, J. D., Minikin, A., and Coe, H.: Black carbon measurements in the boundary layer over western and northern Europe, Atmos. Chem. Phys., 10, 9393–9414, doi:10.5194/acp-10-9393-2010, 2010.

Metcalf, A. R., Craven, J. S., Ensberg, J. J., Brioude, J., Angevine, W., Sorooshian, A., Duong, H. T., Jonsson, H. H., Flagan, R. C., and Seinfeld, J. H. C.-D.: Black carbon aerosol over the Los Angeles Basin during CalNex, J. Geophys. Res., 117, D00V13, doi:10.1029/2011jd017255, 2012.

Moteki, N. and Kondo, Y.: Effects of mixing state on black carbon measurements by laser-induced incandescence, Aerosol Sci. Tech., 41, 398–417, doi:10.1080/02786820701199728, 2007.

Moteki, N. and Kondo, Y.: Method to measure time-dependent scattering cross sections of particles evaporating in a laser beam, J. Aerosol Sci., 39, 348–364, doi:10.1016/j.jaerosci.2007.12.002, 2008.

Moteki, N., Kondo, Y., Miyazaki, Y., Takegawa, N., Komazaki, Y., Kurata, G., Shirai, T., Blake, D. R., Miyakawa, T., and Koike, M.: Evolution of mixing state of black carbon particles: aircraft measurements over the western Pacific in March 2004, Geophys. Res. Lett., 34, L11803, doi:10.1029/2006gl028943, 2007.

Moteki, N., Kondo, Y., and Nakamura, S.: Method to measure refractive indices of small nonspherical particles: application to black carbon particles, J. Aerosol Sci., 41, 513–521, doi:10.1016/j.jaerosci.2010.02.013, 2010.

Moteki, N., Kondo, Y., Oshima, N., Takegawa, N., Koike, M., Kita, K., Matsui, H., and Kajino, M.: Size dependence of wet removal of black carbon aerosols during transport from the boundary layer to the free troposphere, Geophys. Res. Lett., 39, L13802, doi:10.1029/2012GL052034, 2012.

AMTD
7, 5491–5532, 2014

Onasch, T. B., Trimborn, A., Fortner, E. C., Jayne, J. T., Kok, G. L., Williams, L. R., Davidovits, P., and Worsnop, D. R.: Soot Particle Aerosol Mass Spectrometer: development, validation, and initial application, Aerosol Sci. Tech., 46, 804–817, doi:10.1080/02786826.2012.663948, 2012.

Park, K., Kittelson, D. B., Zachariah, M. R., and McMurry, P. H.: Measurement of inherent material density of nanoparticle agglomerates, J. Nanopart. Res., 6, 267–272, doi:10.1023/B:NANO.0000034657.71309.e6, 2004.

Pena, O. and Pal, U.: Scattering of electromagnetic radiation by a multilayered sphere, Comput. Phys. Commun., 180, 2348–2354, doi:10.1016/j.cpc.2009.07.010, 2009.

Petzold, A., Ogren, J. A., Fiebig, M., Laj, P., Li, S.-M., Baltensperger, U., Holzer-Popp, T., Kinne, S., Pappalardo, G., Sugimoto, N., Wehrli, C., Wiedensohler, A., and Zhang, X.-Y.: Recommendations for reporting "black carbon" measurements, Atmos. Chem. Phys., 13, 8365–8379, doi:10.5194/acp-13-8365-2013, 2013.

Ramanathan, V. and Carmichael, G.: Global and regional climate changes due to black carbon, Nat. Geosci., 1, 221–227, doi:10.1038/ngeo156, 2008.

Sahu, L. K., Kondo, Y., Moteki, N., Takegawa, N., Zhao, Y., Cubison, M. J., Jimenez, J. L., Vay, S., Diskin, G. S., Wisthaler, A., Mikoviny, T., Huey, L. G., Weinheimer, A. J., and Knapp, D. J.: Emission characteristics of black carbon in anthropogenic and biomass burning plumes over California during ARCTAS-CARB 2008, J. Geophys. Res., 117, D16302, doi:10.1029/2011JD017401, 2012.

Schnaiter, M., Linke, C., Mohler, O., Naumann, K. H., Saathoff, H., Wagner, R., Schurath, U., and Wehner, B. C.-D.: Absorption amplification of black carbon internally mixed with secondary organic aerosol, J. Geophys. Res., 110, D19204, doi:10.1029/2005jd006046, 2005.

Schwarz, J. P., Gao, R. S., Spackman, J. R., Watts, L. A., Thomson, D. S., Fahey, D. W., Ryerson, T. B., Peischl, J., Holloway, J. S., Trainer, M., Frost, G. J., Baynard, T., Lack, D. A., de Gouw, J. A., Warneke, C., and Del Negro, L. A.: Measurement of the mixing state, mass, and optical size of individual black carbon particles in urban and biomass burning emissions, Geophys. Res. Lett, 35, L13810, doi:10.1029/2008gl033968, 2008a.

Schwarz, J. P., Spackman, J. R., Fahey, D. W., Gao, R. S., Lohmann, U., Stier, P., Watts, L. A., Thomson, D. S., Lack, D. A., Pfister, L., Mahoney, M. J., Baumgardner, D., Wilson, J. C., and Reeves, J. M. C.-D.: Coatings and their enhancement of black carbon light absorption in the tropical atmosphere, J. Geophys. Res., 113, D03203, doi:10.1029/2007jd009042, 2008b.

AMTD
7, 5491–5532, 2014

Schwarz, J. P., Stark, H., Spackman, J. R., Ryerson, T. B., Peischl, J., Swartz, W. H., Gao, R. S., Watts, L. A., and Fahey, D. W. C.-L.: Heating rates and surface dimming due to black carbon aerosol absorption associated with a major US city, Geophys. Res. Lett., 36, L15807, doi:10.1029/2009gl039213, 2009.

Schwarz, J. P., Spackman, J. R., Gao, R. S., Perring, A. E., Cross, E., Onasch, T. B., Ahern, A., Wrobel, W., Davidovits, P., Olfert, J., Dubey, M. K., Mazzoleni, C., and Fahey, D. W.: The Detection Efficiency of the Single Particle Soot Photometer, Aerosol Sci. Tech., 44, 612–628, doi:10.1080/02786826.2010.481298, 2010.

Shiraiwa, M., Kondo, Y., Moteki, N., Takegawa, N., Miyazaki, Y., and Blake, D. R.: Evolution of mixing state of black carbon in polluted air from Tokyo, Geophys. Res. Lett., 34, L16803, doi:10.1029/2007gl029819, 2007.

Shiraiwa, M., Kondo, Y., Moteki, N., Takegawa, N., Sahu, L. K., Takami, A., Hatakeyama, S., Yonemura, S., and Blake, D. R.: Radiative impact of mixing state of black carbon aerosol in Asian outflow, J. Geophys. Res., 113, D24210, doi:10.1029/2008jd010546, 2008.

Shiraiwa, M., Kondo, Y., Iwamoto, T., and Kita, K.: Amplification of light absorption of black carbon by organic coating, Aerosol Sci. Tech., 44, 46–54, doi:10.1080/02786820903357686, 2010.

Slowik, J. G., Cross, E. S., Han, J. H., Davidovits, P., Onasch, T. B., Jayne, J. T., Williams, L. R., Canagaratna, M. R., Worsnop, D. R., Chakrabarty, R. K., Moosmuller, H., Arnott, W. P., Schwarz, J. P., Gao, R. S., Fahey, D. W., Kok, G. L., and Petzold, A.: An inter-comparison of instruments measuring black carbon content of soot particles, Aerosol Sci. Tech., 41, 295–314, doi:10.1080/02786820701197078, 2007.

Stelson, A. W.: Urban aerosol refractive-index prediction by partial molar refraction approach, Environ. Sci. Technol., 24, 1676–1679, doi:10.1021/es00081a008, 1990.

Stephens, M., Turner, N., and Sandberg, J.: Particle identification by laser-induced incandescence in a solid-state laser cavity, Appl. Optics, 42, 3726–3736, 2003.

Subramanian, R., Kok, G. L., Baumgardner, D., Clarke, A., Shinozuka, Y., Campos, T. L., Heizer, C. G., Stephens, B. B., de Foy, B., Voss, P. B., and Zaveri, R. A.: Black carbon over Mexico: the effect of atmospheric transport on mixing state, mass absorption cross-section, and BC/CO ratios, Atmos. Chem. Phys., 10, 219–237, doi:10.5194/acp-10-219-2010, 2010.

Taylor, J. W., Allan, J. D., Liu, D., Flynn, M., Hayes, P. L., Jimenez, J. L., Lefer, B. L., Grossberg, N., Flynn, J., Gilman, J., de Gouw, J. A., and Coe, H.: Comparison of measured black

AMTD
7, 5491–5532, 2014

carbon mass absorption coefficient to modelled values during CalNex 2010, J. Geophys. Res.-Atmos., in preparation, 2014.
Washenfelder, R. A., Young, C. J., Brown, S. S., Angevine, W. M., Atlas, E. L., Blake, D. R., Bon, D. M., Cubison, M. J., de Gouw, J. A., Dusanter, S., Flynn, J., Gilman, J. B., Graus, M., Griffith, S., Grossberg, N., Hayes, P. L., Jimenez, J. L., Kuster, W. C., Lefer, B. L., Pollack, I. B., Ryerson, T. B., Stark, H., Stevens, P. S., and Trainer, M. K. C.-D.: The glyoxal budget and its contribution to organic aerosol for Los Angeles, California, during CalNex 2010, J. Geophys. Res., 116, D00V02, doi:10.1029/2011jd016314, 2011.
Weast, R. C.: CRC Handbook of Chemistry and Physics, 58th Edn., CRC Press, Cleveland, Ohio, USA ET-58, 1977.
Yang, W.: Improved recursive algorithm for light scattering by a multilayered sphere, Appl. Optics, 42, 1710–1720, 2003.
Zhang, R., Khalizov, A. F., Pagels, J., Zhang, D., Xue, H., and McMurry, P. H.: Variability in morphology, hygroscopicity, and optical properties of soot aerosols during atmospheric processing, P. Natl. Acad. Sci. USA, 105, 10291–10296, doi:10.1073/pnas.0804860105, 2008.

AMTD
7, 5491–5532, 2014

Table 1. Summary of core densities and refractive indicies used in previous SP2 core/shell calculations.

Core density (ρ_C, g cm^3)	Reference	Core refractive index n_C	Reference	Studies used
1.8	Bond and Bergstrom (2006)	(2.26 – 1.26i)	Moteki et al. (2010)	This study (Laborde et al., 2013)
1.8	Bond and Bergstrom (2006)	(1.95 – 0.79i)	Bond and Bergstrom (2006)	Langridge et al. (2012), Metcalf et al. (2012)
1.9	Bond and Bergstrom (2006)	(1.95 – 0.79i)	Bond and Bergstrom (2006)	Subramanian et al. (2010)
1.77	Park et al. (2004)	(1.87 – 0.56i)	Marley et al. (2001)	Shiraiwa et al. (2008)
2		(2 – 1i)	Schnaiter et al. (2005)	Schwarz et al. (2008a, b, 2009)
2	Hess et al. (1998)	(1.76 – 0.44i)	Hess et al. (1998)	Kondo et al. (2011a)*, Moteki et al. (2012)*, Sahu et al. (2012)*

* These studies used the scattering-only technique to derive coating thickness, but the values are included here for comparison.

AMTD
7, 5491–5532, 2014

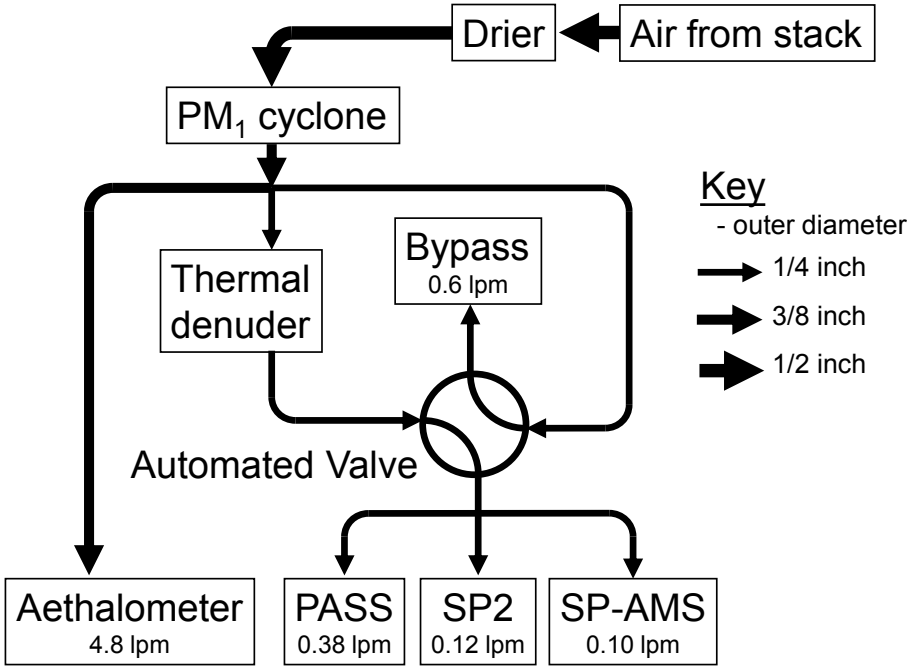

Figure 1. Schematic of the sampling system used for the University of Manchester BC instruments during CalNex, showing the instruments' sample flows. Stainless steel Y-pieces were used when splitting flows. Before the thermodenuder and bypass flow were setup, the Aethalometer flow rate was 5.4 L min^{-1} to ensure sufficient flow through the cyclone.

AMTD
7, 5491–5532, 2014

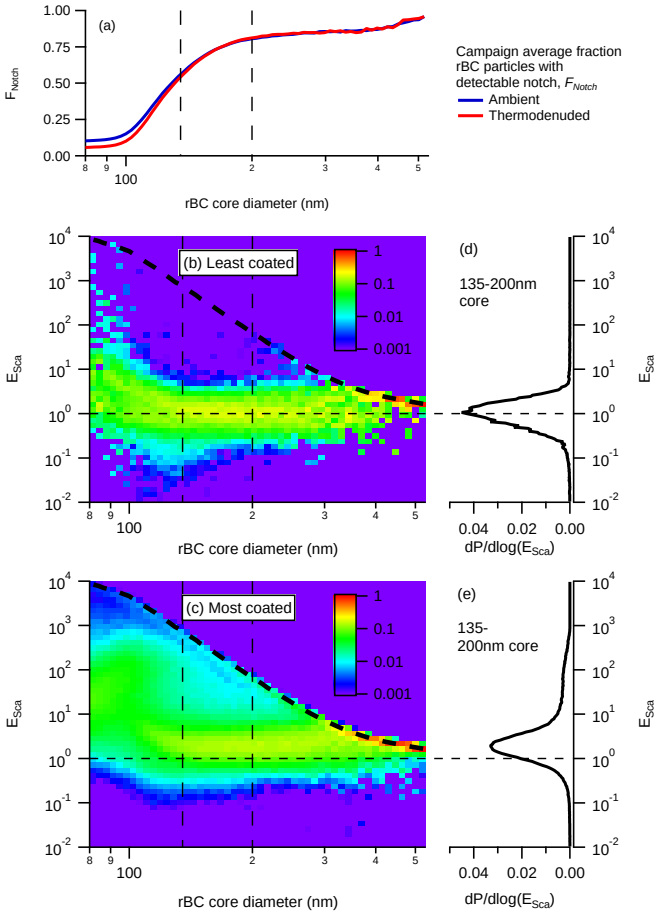

AMTD
7, 5491–5532, 2014

Sensitivity assessment of SP2 core/shell parameters

J. W. Taylor et al.

Figure 2. Diagnostics for determining the range of rBC core diameter used for Mie modelling. **(a)** shows the fraction of BC-containing particles with detectable notch positions, averaged over the whole campaign, as a function of D_C. **(b)** and **(c)** show probability density functions, $dP/d\log(E_{Sca})$ for each core diameter bin, under the least processed (particles drawn through the thermodenuder $> 220\,^{\circ}C$ and $-\log(NO_x/NO_y) <$ 10th percentile) and most processed (direct inlet and $-\log(NO_x/NO_y) >$ 90th percentile) conditions respectively. The thick dashed black lines represent the calculated saturation of the scattering detector at 5 % of maximum laser intensity. **(d)** and **(e)** are $dP/d\log(E_{Sca})$ distributions for particles in the range $0.135 \leq D_C < 0.2\,\mu m$, bordered by the vertical dashed lines. The horizontal dashed lines show a core scatter ratio of 1. Figure 2b and c are scaled in arbitrary units, and are normalized such that each column, sums to 1. **(d)** and **(e)** are also normalized to sum to 1, though they are distributions over the range $0.135 \leq D_C < 0.2\,\mu m$, rather than averages of **(b)** and **(c)**, and are thus weighted more heavily towards the smaller particles within the range. **(b–e)** were calculated assuming $\rho_C = 1.8\,g\,cm^{-3}$ and $n_C = (2.26 - 1.26i)$.

AMTD
7, 5491–5532, 2014

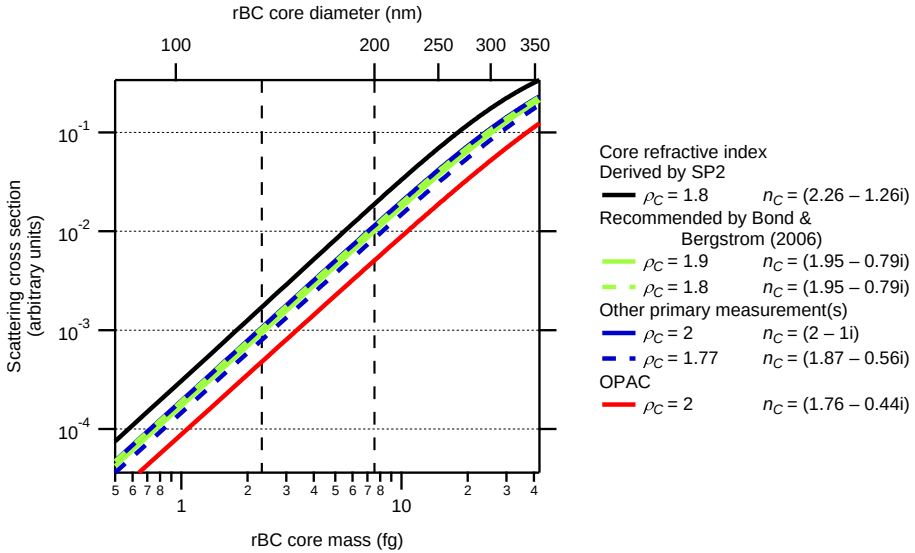

Figure 3. Calculated scattering cross section, integrated over the angles of the SP2's scatter detectors, for the different combinations of density and refractive index used in previous SP2 ambient core/shell modelling. Densities are in units of g cm^{-3}. The vertical dashed lines bound the range of core diameter used for coating calculations in this study.

AMTD
7, 5491–5532, 2014

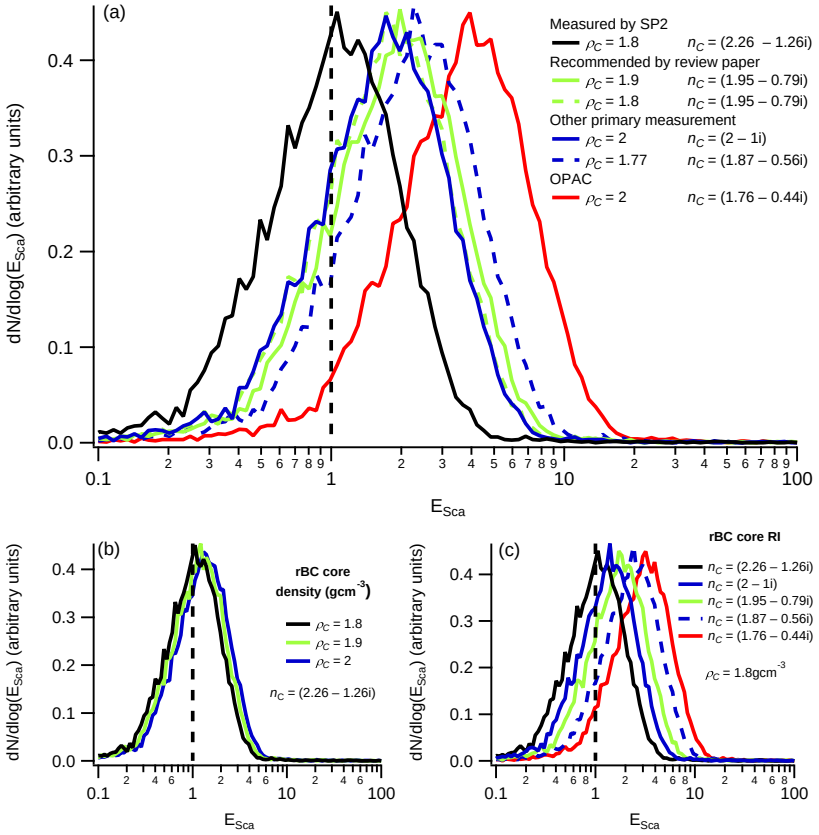

Figure 4. Normalized E_{Sca} distribution for the least coated particles (thermodenuder > 220 °C and $-\log(NO_x/NO_y)$ < 10th percentile) for different rBC core densities and refractive indices. **(a)** shows data for density (in units of g cm^{-3}) and refractive index combinations used in previous SP2 core/shell modelling, whilst **(b)** and **(c)** illustrate the sensitivity to core density and refractive index respectively.

AMTD
7, 5491–5532, 2014

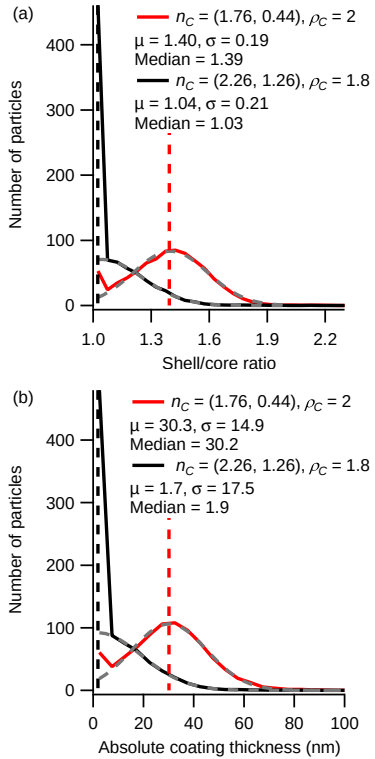

Figure 5. Distributions of **(a)** relative and **(b)** absolute coating thickness, measured under the same conditions as Fig. 4. The dashed grey lines are Gaussian fits to the distributions, and fit parameters are listed in the legend. The first bin represents all particles with $E_{Sca} \leq 1$, and this bin was not used in the Gaussian fits. The vertical dashed lines are the median values, also listed in the legend. These are often used to compare changes in coatings and are only biased by particles with $E_{Sca} < 1$ if the median value falls in this range.

AMTD
7, 5491–5532, 2014

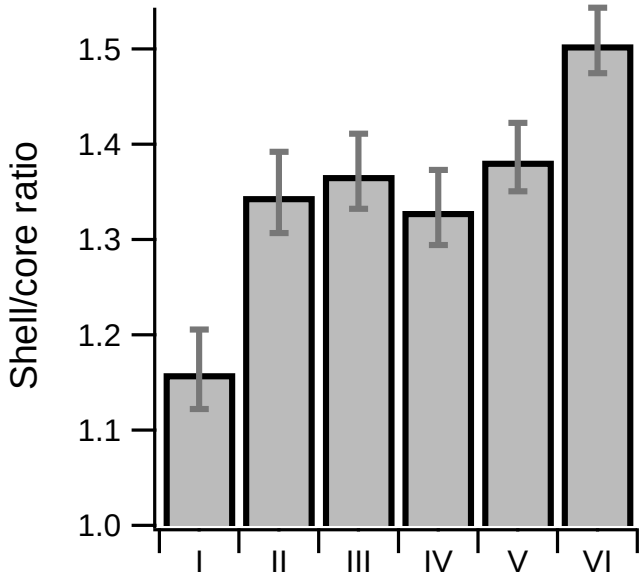

Key

I	$n_C = (2.26 - 1.26i)$	$\rho_C = 1.8$
II	$n_C = (2 - 1i)$	$\rho_C = 2$
III	$n_C = (1.95 - 0.79i)$	$\rho_C = 1.8$
IV	$n_C = (1.95 - 0.79i)$	$\rho_C = 1.9$
V	$n_C = (1.87 - 0.56i)$	$\rho_C = 1.77$
VI	$n_C = (1.76 - 0.44i)$	$\rho_C = 2$

Figure 6. Sensitivity of the median shell/core ratio to rBC core refractive index and density, listed in units of g cm^{-3}. Data shown are the medians of each 5 min period throughout the campaign, with error bars for the 25th and 75th percentiles.

AMTD
7, 5491–5532, 2014

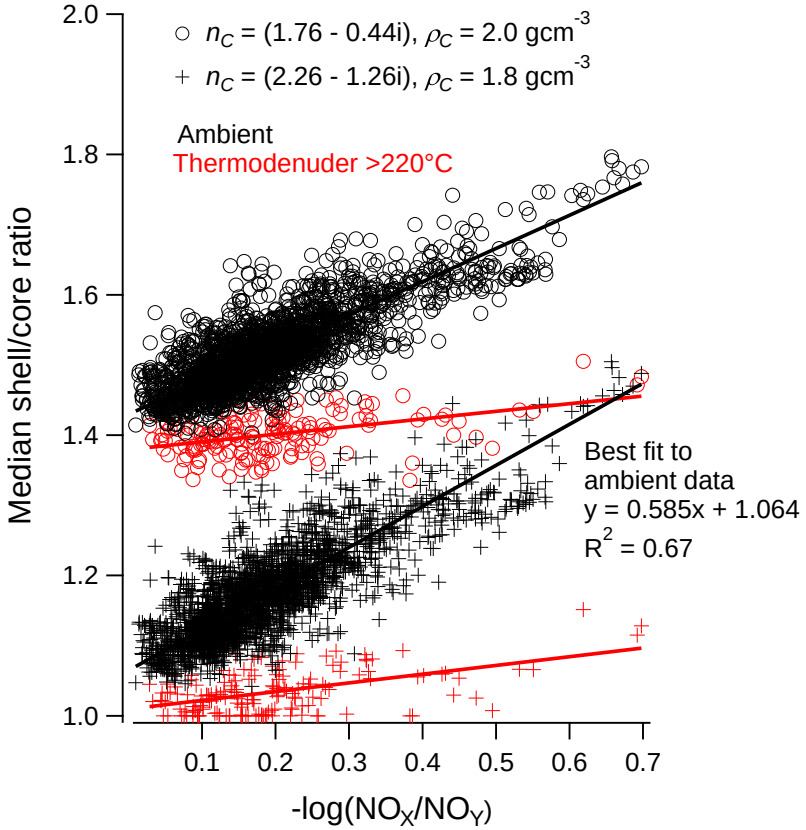

Figure 7. Median shell/core ratio for particles with $135 \leq D_C \leq 200$ nm plotted vs. ambient $-\log(NO_x/NO_y)$. Data are plotted for the sets of core refractive index and density that result in the thickest and thinnest coatings. Both ambient and thermodenuded (> 220 °C) data are shown. The straight lines are linear orthogonal distance regression fits to the data. By definition, the minimum measurable shell/core ratio is 1.

AMTD
7, 5491–5532, 2014